Red-Emission Oligofluorene Electrophosphorescent Diodes Based on Bis[2-(9,9-dihexyl-9*H*-fluoren-2-yl)quinoline-*C*3,*N*]acetylacetonatoiridium(III) and Solvent Treatment for Interface Modification

Juo-Hao Li,[†] Sven Andresen,[‡] Hua-Hsien Liao,[†] and Yang Yang*[,†]

Department of Materials Science and Engineering, University of California, Los Angeles, Los Angeles, California 90095, and Canon Development Americas, Irvine, California 92618

ABSTRACT Efficient solution-processed organic light emitting diodes based on oligofluorene doped with bis[2-(9,9-dihexyl-9*H*-fluoren-2-yl)quinoline-*C*3,*N*]- acetylacetonatoiridium(III) [Ir(C6flq)$_2$(acac)] have been demonstrated. The oligofluorene and [Ir(C6flq)$_2$(acac)] show excellent solubility and processibility, with a device performance of 7.83 ± 0.52 cd A^{-1} and 3.30 ± 0.10 lm W^{1-} at 2479 ± 45 cd m^{-2} brightness with Commission International de L'Eclairage coordinates (0.66, 0.33). It was discovered that the efficiency can be further enhanced by exposing the finished organic thin film to a polar solvent or solvent vapor before deposition of the cathode contact. As a result, a peak efficiency of 12.20 ± 0.16 cd A^{-1} and 6.35 ± 0.03 lm W^{1-} at 1821 ± 238 cd m^{-2} brightness is achieved. This efficiency enhancement can be attributed to the presence of interface dipoles between the light-emitting layer and cathode contact.

KEYWORDS: PLEDs • phosphorescence • organic light-emitting diodes

INTRODUCTION

Electrophosphorescent organic light-emitting diodes (OLEDs) have shown attractive characteristics because of their high efficiency compared to OLEDs using fluorescent materials in the emitting layer (1−7). Recently, significant improvements of device efficiency and lifetime have further accelerated the development of applications in the fields of display and solid-state lighting (8, 9). Solution-processed OLEDs have shown the advantage of simple and cost-effective fabrication. However, the progress in solution-processed electrophosphorescent diodes has often been limited because of lack of suitable host materials. The primary requirement for host materials is good solubility and processibility to form high-quality thin films with tens of nanometers thickness. Also, the material electronic structure, such as the lowest unoccupied molecular orbital (LUMO) and highest occupied molecular orbital (HOMO) levels, plays an important role in the charge transport and energy transfer in a blend system. Energy transfer from host to triplet dopants can occur through Förster (dipole−dipole coupling) or Dexter (exchange of electrons) processes (10). Efficient energy transfer can occur when the energy levels of the host and dopant are properly aligned (11). Therefore, well-designed host materials and suitable triplet dopants are both equally necessary for efficient solution-processed electrophosphorescent OLEDs. On the other hand, from the viewpoint of device physics, the device efficiency is highly dependent on the interface between the emission layer and electrode. Properly balanced injection of electrons and holes can significantly improve the light output and device efficiency (12). Hence, the interface engineering is also an important subject in OLED research.

Our previous work (3) showed two kinds of tris(1-phenylisoquinolinato-*C*2,*N*)iridium(III) derivatives having high efficiency in PLEDs based on the polyfluorene host material. In this work, our strategy is to use a blend system with a blue-emission oligofluorene host and a red-emission iridium complex triplet dopant. Not only was the alignment of energy-level and energy-transfer processes examined by the position of the LUMO and HOMO levels and the triplet energy, but also the absorption and photoluminance (PL) spectra were taken to show the compatibility of the host and dopant materials in this blend system. In addition, a simple and effective interface modification by solvent treatment was discovered to have a significant influence on the device performance. An efficiency of 12.20 ± 0.16 cd A^{-1} and 6.35 ± 0.03 lm W^{-1} at 1821 ± 238 cd m^{-2} brightness was obtained. Several techniques were applied to investigate the mechanism of this enhancement: the built-in potential of the finished device was measured by electroabsorption (EA) spectroscopy; X-ray photoelectron spectroscopy (XPS/UPS) was used to investigate the electronic structure of the surface of the active layer before and after the treatment. Results indicated a reduction of the barrier height because of the

* To whom correspondence should be addressed. E-mail: yangy@ucla.edu.
Received for review August 20, 2008 and accepted October 3, 2008
[†] University of California, Los Angeles.
[‡] Canon Development Americas.
DOI: 10.1021/am8000133

Published on Web 11/24/2008

existence of interface dipoles. Finally, atomic force microscopy (AFM) analyses revealed the important role of the dopant on the surface morphology in our blend system.

EXPERIMENTAL SECTION

Device fabrication started from a precleaned indium−tin oxide (ITO) substrate, which underwent a routine cleaning procedure including sonication in detergent followed by repeated rinsing in deionized water, acetone, and isopropyl alcohol, and finally treatment with ultraviolet (UV) ozone. A layer of conductive polymer PEDOT/PSS (Baytron-P 4083) was spun onto the substrate as a hole transport layer at a spin speed of 4000 rpm. The PEDOT/PSS layer was then baked at 120 °C for 30 min to remove residual water. The light-emitting layer (LEL) was prepared from xylene solutions of pure oligofluorene or from oligofluorene doped with 1−8 wt % $Ir(C6flq)_2(acac)$. After spin coating, the LEL film was baked at 70 °C for 30 min. Solvent treatment was carried out after the baking procedure, and acetonitrile was used for all of the data in this manuscript. The solvent can be directly dropped on top of the LEL surface and dried by spin coating at 3000 rpm for 60 s. Solvent treatment can also be done by exposing the surface to solvent vapor for 20 min in a container. All of the solution processes except the preparation of the PEDOT/PSS layer were performed in a nitrogen-atmosphere glovebox. After solvent treatment, the substrates were transferred into a deposition chamber. Then the cathode materials were thermally evaporated under a vacuum of 1×10^{-6} Torr. PL spectra were measured with a Jobin Yvon Spex Fluorolog-3 double-grating spectrofluorometer. Electroluminance (EL) and the Commission International de L'Eclairage (CIE) coordinates were measured with a Spectrascan PR 650. All devices were tested in a nitrogen environment. The EA spectrometer consisted of a Oriel xenon lamp, a Acton Spectropro 2150 monochromator, a low-noise photodetector, a Keithley 2400 sourcemeter, and a Stanford SR830 lock-in amplifier. The direct current (dc) and alternating current (ac) bias outputs were fed into a summing amplifier used as the alternating voltage source. A sinusoidal voltage of 2 kHz frequency was applied across the two electrodes of the diode. The monochromatized beam was focused onto the sample through the glass substrate at ∼45° incidence, reflected off the metal electrode after traveling through the polymer, and finally collected by a lens and focused onto the silicon photodiode. The photodetector output consisted of a dc (T) and an ac (ΔT) component, and the ratio of the two gives the EA signal $\Delta T/T$. The XPS and UPS experiments were carried out in an Omicron Nanotechnology system with a base pressure of 2×10^{-10} Torr. UPS spectra were obtained using the HeI line ($h\nu = 21.2$ eV); a Mg Kα radiation source ($h\nu = 1253.6$ eV) was used for the XPS measurements. Samples were biased at −5 V during UPS measurements to observe the secondary electron edge. For surface morphology measurement, samples were examined by A Digital Instruments Multimode scanning probe microscope under an ambient air atmosphere. The height, three dimensions, and phase images were captured, and the surface roughness was obtained by using the affiliated software.

RESULTS AND DISCUSSION

A. Material Characteristics of the Blend System. The chemical structure of $Ir(C6flq)_2(acac)$ is shown in Figure 1a (13). $Ir(C6flq)_2(acac)$ can be easily dissolved in common organic solvents such as xylene and chlorobenzene. Figure 1b shows the UV−visible absorption spectrum of the dopant and the PL spectra of the host material and phosphorescent dopant. As can be seen, there is a noteable overlap between the absorption spectrum of the dopant and the emission

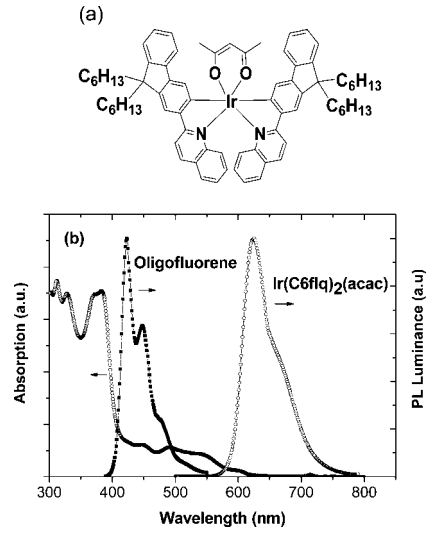

FIGURE 1. (a) Chemical structure of the triplet dopant, $Ir(C6flq)_2(acac)$, and (b) UV−visible absorption of $Ir(C6flq)_2(acac)$ and PL spectra of the host and dopant. There is an overlap area between the absorption of the dopant and the PL spectrum of the host.

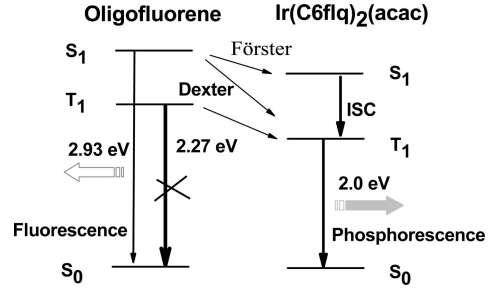

FIGURE 2. Schematic diagram for energy-level alignment and energy-transfer process between the oligofluorene host and the $Ir(C6flq)_2(acac)$ dopant.

spectrum of the host, indicating that efficient Förster energy transfer can occur in this blend system.

The energy-transfer process can be further explained with the energy-level alignment of host and dopant materials. The LUMO and HOMO levels of the oligofluorene were measured to be 2.86 ± 0.05 and 5.83 ± 0.03 eV, respectively. For the iridium complex, 3.21 ± 0.03 eV for the LUMO and 5.33 ± 0.04 eV for the HOMO were found. Figure 2 shows the energy-level diagram and possible pathways for the energy transfer between the oligofluorene host and the $Ir(C6flq)_2$-(acac) dopant. Effective Förster and energy transfer can occur from the singlet state of the oligofluorene to the lower lying singlet or triplet states of the dopant. Furthermore, energy transfer can take place between the T_1 level of the host and dopant and via intersystem crossing between the S_1 and T_1 states of the dopant. Because the T_1 level of the host lies about 0.27 eV higher than that of the dopant, back transfer of energy between the two triplet states cannot occur. Therefore, efficient red emission from the dopant can be expected for this host−dopant combination.

B. Electrophosphorescent Device Performance and Solvent Treatment. In this work, a simple architecture consisting of a spin-coated LEL sandwiched by electrodes was employed to fabricate our OLEDs. Our previous studies (3, 12) indicate that highly efficient electrophospho-

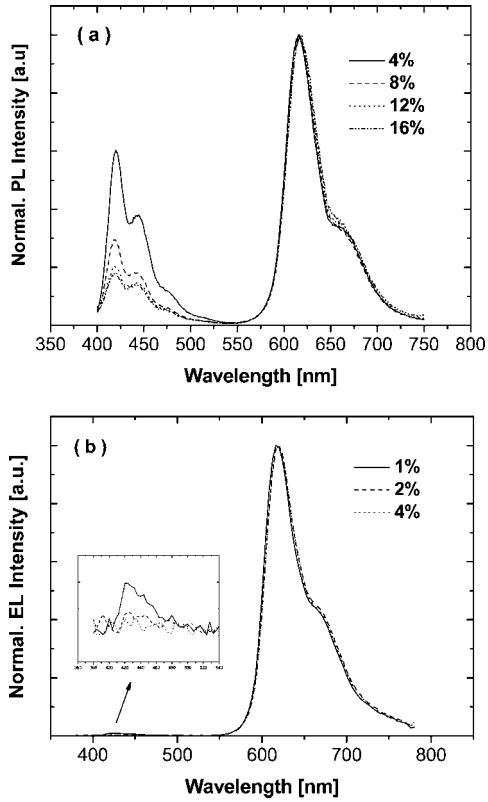

FIGURE 3. PL (a) and (b) EL spectra of the oligofluorene: $Ir(C6flq)_2(acac)$ blend with different dopant concentrations. In comparison, it only needs 1−2% for EL devices to complete the energy transfer, suggesting that charge trapping occurred in the blend system.

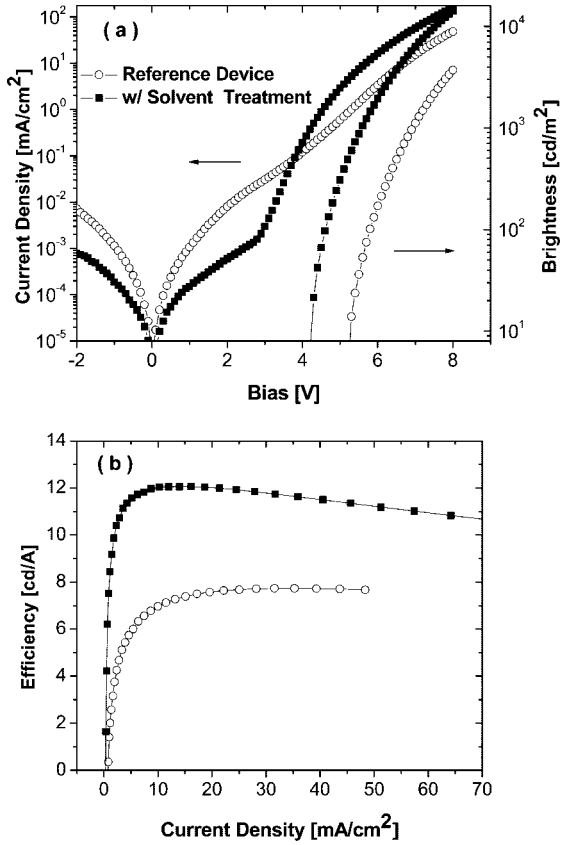

FIGURE 4. $J-V-L$ characteristics (a) and current efficiency (b) of oligofluorene-blended devices with and without solvent treatments. Device structure: ITO/PEDOT/LEP/Cs_2CO_3/Al.

rescent OLEDs can be obtained by optimizing the dopant concentration as well as the thickness of cesium carbonate (Cs_2CO_3) and the LEL. The PL spectra in Figure 3a show that an optimum energy transfer occurred at the 12−16 wt % doping level. This suggests that Dexter transition, which is a short-range transfer process, may play an important part in the photoexcitation process. The EL spectra show that the blue emission from the host disappears at significantly lower doping levels. A dopant concentration of only 1−2 wt % is sufficient to completely suppress the host emission. We relate this observation to direct trapping of both the holes and electrons in the device.

Charge balance is another important strategy for a high device performance. This can be achieved by optimizing the thickness of the Cs_2CO_3 layer to reduce the barrier height for electron injection (12). After optimization of the doping concentration and the thickness of the Cs_2CO_3 layer, efficient red-emitting electrophosphorescent diodes were achieved. The current density−voltage−luminance ($J-V-L$) characteristics and the EL spectrum are shown in parts a and c of Figure 4. A peak efficiency of 7.83 ± 0.52 cd A^{-1} and 3.30 ± 0.10 lm W^{-1} at 2479 ± 45 cd m^{-2} brightness was obtained. The CIE coordinates were (0.66, 0.33), as shown in Figure 4b.

Except for variation of the Cs_2CO_3 thickness to reduce the electron-injection barrier, it was interesting to find that the efficiency can be further enhanced by solvent treatment of the polymer film prior to thermal deposition of the metal electrode. The treatment was performed by exposure of the surface of the active layer to a solvent vapor for a short period of time or by direct solvent deposition on top of the surface and then drying by spin coating. The details can be found in the Experimental Section. As shown in Figure 4a, the $J-V-L$ characteristics of the device that underwent solvent treatment show a significant improvement compared with the untreated device. We obtained an efficiency of 12.20 ± 0.16 cd A^{-1} and 6.31 ± 0.03 lm W^{-1} at 1821 ± 238 cd m^{-2} brightness with CIE coordinates (0.66, 0.33). To realize if the effects of the solvent treatment on the device performance are also applicable to other light-emitting polymers, PLEDs with different active polymers were constructed and the $I-V$ characteristics were compared for this purpose. Figure 5a shows that the solvent treatment also has effects on PLEDs with active polymers such as poly[2-methoxy-5(2-ethylhexyloxyphenylenevinylene)] (MEH-PPV), poly(9,9-dioctylfluorene) (PFO), and PF/poly(9,9-dioctylfluorene-*co*-benzothiadiazole) (GPF). The current density of the devices increases significantly after solvent treatment is employed on the surface of the active layer. Furthermore, several polar solvents are chosen to investigate the solvent dependence. Similar effects are observed in the increase of the current density in green PLEDs with these polar solvents, as shown in Figure 5b. It is important to select a solvent that does not dissolve or damage the polymer layer underneath. It is apparent from the observation above that the solvent treatment has vital influences on the device performance,

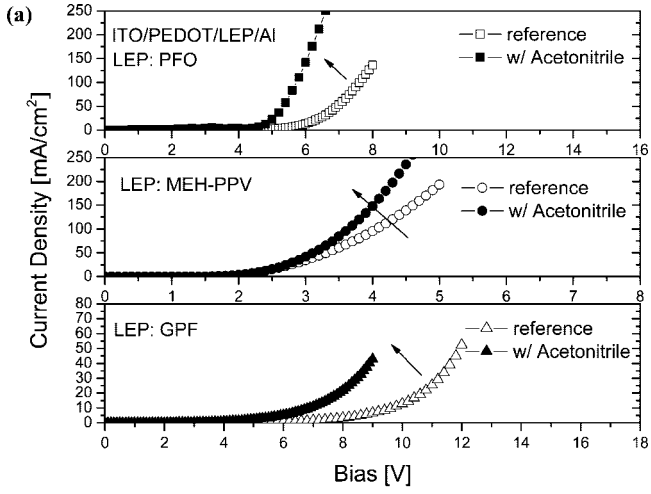

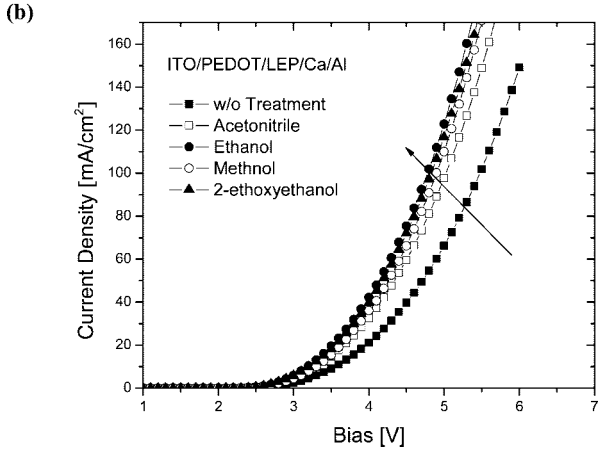

FIGURE 5. (a) Polymer and (b) solvent dependences on the $J-V$ characteristics of PLEDs using solvent treatment as an interface modification. The current density of PLEDs shows an increase when solvent treatment is applied on the surface of an active polymer before evaporation of the metal cathode.

and the following question will be the origin of the influences due to the solvent treatment.

First, one would wonder whether the material properties will change after the solvent treatment applied on the surface of the polymers. The basic characteristics of the emitting layer and electrophosphorescent devices, such as UV−visible absorption and EL spectra, were examined and found not change after the solvent treatment, as shown in Figure 6. This suggests that neither a change in the chemical structure of the active layer nor a change in the emission mechanism is responsible for the improvements. If the basic properties of the active layer have not been changed, then the most likely reason responsible for the increased efficiency should remain at the interface. Therefore, surface and interface analyses were conducted by XPS/UPS, AFM, and EA spectroscopy to study the effect of the solvent treatment on the interface between the LEL and cathode.

C. EA Spectroscopy and Built-in Potential. One way to study the effect of the solvent treatment on the interface between the active layer and cathode is to examine the energy-level line-up of the finished diodes. EA spectroscopy is a noninvasive and direct technique that can provide information on the built-in potential (V_{bi}) across the active

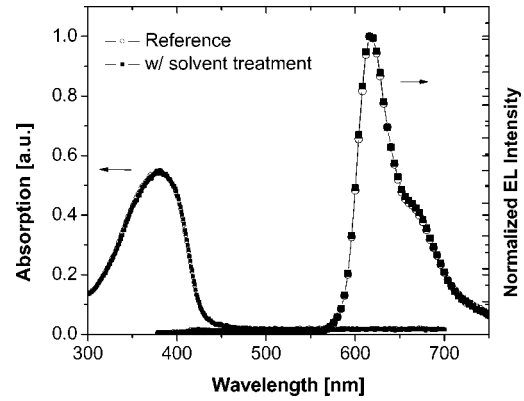

FIGURE 6. EL and UV−visible absorption spectra of PLEDs with and without solvent treatment. No obvious change is observed after solvent treatments, indicating that the chemical structure of the materials and the emission mechanism remain unchanged.

layer and any shift of the barrier height while changing the electrodes (14−16). The built-in potential originates from the equilibrium of the Fermi level throughout the device structure. Because our devices have the same anode structure, and the energy band gap (E_g) is an intrinsic property that usually does not change, the variation of V_{bi} can represent a change of the barrier height of the cathode [$e\Delta V_{bi} = -\Delta\Phi$(cathode)]. In short, if the variation of V_{bi} from the measurement of EA signals is known, then a change of the barrier height due to surface modification can be verified.

The undoped oligomer was first examined. In Figure 7a, we show the results of the EA measurement for two different types of cathodes, aluminum (Al) and Cs_2CO_3/Al. V_{bi} obtained for the Al cathode is 1.08 ± 0.11 V, which is consistent with the work-function variation of the electrodes, Al (4.3 eV) and PEDOT (5.2 eV). It is found that V_{bi} increases by around 0.43 ± 0.03 V after solvent treatment. V_{bi} for the cathode consisting of Cs_2CO_3/Al is also found to be increased by 0.18 ± 0.03 V. As described above, the increase of the built-in potential suggests that a reduction in the cathode barrier height [$e\Delta V_{bi} = -\Delta\Phi$(cathode)] occurs. For the doped devices, a similar trend is found for a shift of the built-in potential before and after the solvent treatment. On the other hand, it is also noticed that the shift of the built-in potential varies for different cathodes. The metal dependence is important and will be discussed in the next section. It is worth noticing that the shift of the built-in voltage seems small compared with the improvement of the device performance. This is because ΔV_{bi} only reflects the reduction of the barrier energy at the interface, resulting in more efficient electron injection. However, the charge balance actually should be attributed to the reason for the improvement. If one looks at the $J-V-L$ characteristics (Figure 4), the current density and brightness increase dramatically after the turn-on of the device, indicating that more charge recombination is taking place and generating more photons inside the light-emitting layer.

It is highly desirable to understand the origin of the barrier reduction because the materials of the electrodes and the emission layer remain unchanged in this case. So, the possible explanation for the shift of the built-in potential

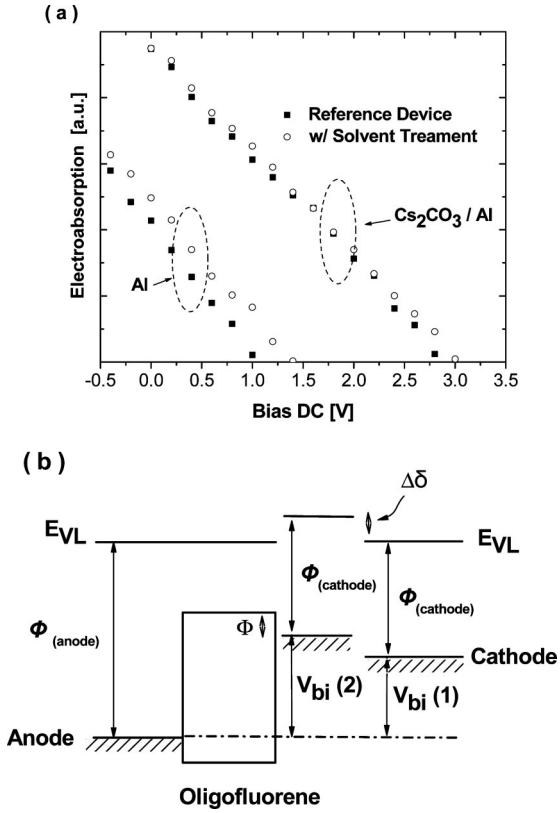

FIGURE 7. (a) EA response at $\lambda = 420$ nm and $V_{ac} = 0.5$ V as a function of the applied dc bias for the oligofluorene LEDs with Al and Cs_2CO_3/Al cathodes and a comparison of the solvent treatment for each cathode. The built-in potential (V_{bi}) is determined by the EA response intersecting the horizontal $y = 0$ axis. (b) Schematic diagram of the built-in potential before [$V_{bi}(1)$] and after [$V_{bi}(2)$] solvent treatment and the existence of interface dipoles ($\Delta\delta$).

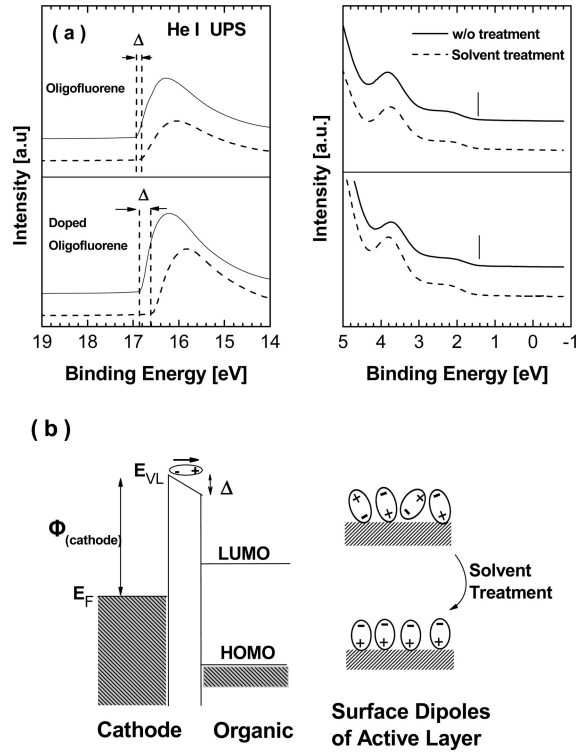

FIGURE 8. (a) UPS spectra of undoped and doped oligofluorene. The left-hand side shows the shift (Δ) of the vacuum level (E_{VL}) after solvent treatment, and the right-hand side corresponds to the HOMO region. (b) Schematic diagram of the energy-level alignment between the cathode and organic layer. The shift of E_{VL} suggests the presence of interface dipoles, the direction is toward the surface of the organic material, and a model shows a change of the orientation of the surface dipole after solvent treatment.

should be ascribed to the interface between the cathode and the active layer. Alternatively, the alignment of the energy levels throughout the device can be generally expressed as (16)

$$eV_{bi} = \phi(\text{anode}) - \phi(\text{cathode}) - \delta \qquad (1)$$

where ϕ represents the work function of the electrodes and δ is the interface dipoles. Therefore, the shift of the built-in potential suggests the presence of interface dipoles ($e\Delta V_{bi} = -\Delta\delta$) because no change of the work function occurs in this case. Figure 7b shows a schematic diagram to explain the existence of interface dipoles in the device. It is clear to see that $V_{bi}(2)$ increases after solvent treatment, the barrier height (Φ) for charge injection decreases, and the difference of V_{bi} implies the existence of interface dipoles. More evidence and direct measurement are needed to further prove the existence of interface dipoles. Therefore, to address the questions of how the interface dipoles are generated and how they relate to the solvent treatment, surface analyses were conducted by XPS/UPS.

D. XPS and UPS Studies of the Interface. XPS/UPS is an important and powerful technique for surface analysis (17−20), including the composition analysis and interfacial electronic structure. We compare the surface energy state of the thin film before and after solvent treatment by using the UPS. The oligomer layer was prepared in a nitrogen atmosphere. The light source is a HeI discharge of $h\nu = 21.2$ eV. Figure 8a shows the UPS spectra for pure and doped oligomer thin films before and after solvent treatment. The left-hand cutoff obtained from the secondary photoelectrons represents the movementof the surface vacuum level (E_{VL}), and the right-hand onset corresponds to the HOMO region of organic materials. In Figure 8a, it is clear to see that both pure and doped oligomers show a shift of the vacuum level after solvent treatment, while no obvious change or new peak was observed near the HOMO region, indicating that no new surface state was formed through surface treatment. The diagram in Figure 8b shows an energy-level alignment between the cathode and the organic active layer. The shift of E_{VL} due to solvent treatment can promote the injection of electrons because the Schottky barrier at the interface between the metal and organic layer is reduced. In addition, it is also noticed that the shift of the vacuum level is larger for doped oligofluorene (0.33 ± 0.02 eV) than for undoped material (0.12 ± 0.02 eV), implying that there could be dopant effects involved, and this will be discussed in the next section.

The shift of E_{VL} reflects a change of the surface properties, such as dipole layer formation, which can result from various origins. Several reasons for the formation of interface dipoles including (a) charge transfer across the interface, (b) image potential-induced polarization of the organic material, (c) pushing back of the electron cloud tailing out of the metal surface by the organic material, (d) chemical reaction, (e)

the existence of interface states, and (f) alignment of the permanent dipole of the organic material have been proposed (17, 20, 21). Among these factors, (a)−(c) more likely occurred under the presence of a metal contact, while in our case, the dipole layer may form before contact with the metal cathode. Chemical reaction and the existence of interface states are not observed from the core-level peaks of XPS results and from the HOMO region of UPS spectra, respectively, after solvent treatment. In addition, no evidence for solvent residues was found during the XPS measurement. Therefore, the surface polarization is more likely responsible for the dipole layer formation. Because the solvents used in this work are of high polarity, a dipole−dipole interaction between the solvent and surface molecules, leading to a change in the orientation of the dipole moment, is very likely. The proposed chemical model is shown in Figure 8b.

On the other hand, the metal contact also plays an important role in the formation of interface dipoles. The metal dependence on the interface dipoles at a metal−organic semiconductor has been proven and given much discussion in the literature (17, 21, 22). It is noticed the shift of the built-in potential will be various if different metal contacts are deposited on the top of the organic material after solvent treatment. Therefore, several factors including organic active materials, types of solvent, and different metal contacts will have significant influences on the formation of interface dipoles. Except the viewpoints of the energy-level alignment and surface composition from XPS/UPS observation, we can also gain further insight into some surface features through other surface analysis techniques such as AFM.

E. Investigation of the Surface Morphology by AFM. The result of UPS shows the effect of the solvent treatment on the shift of E_{VL}, which accounts for the reduction of the barrier height. However, AFM can provide information from the very surface of a thin film, such as morphology and distribution of different phases. Figure 9 shows AFM images of undoped and doped oligomer thin films before and after solvent treatment. It was observed that a second phase appeared in the doped thin film (Figure 9c,d) compared with undoped oligofluorene (Figure 9a,b). An aggregation occurs after applying the solvent treatment, also resulting in an increase of the roughness, as shown in a 3D image (Figure 9e−h). Therefore, this indicates that the effects of the solvent treatment may have more influence on the doped material, which is consistent with the previous observation on the larger shift of the vacuum level in Figure 8a. The role of the dopant in the surface morphology has not been fully understood; however, upon the E_{VL} shift and the increase in the built-in potential in our doped devices, the significance of dopant effects has been revealed in this work.

CONCLUSIONS

This work has shown that the oligofluorene/Ir(C6flq)$_2$(acac) blend can achieve high efficiency for solution-processed OLEDs, revealing the application potential of oligomer OLEDs. The solvent treatment of the LEL provides a simple and effective method to engineer the interface properties and results in an enhancement of the device performance. An efficiency of 12.20 ± 0.16 cd A^{-1} and 6.35 ± 0.03 lm W^{-1} at 1821 ± 238 cd m^{-2} brightness is achieved with CIE coordinates of (0.66, 0.33). The device and EA studies show that the improvement results from the reduction of the barrier height for electron injection, proven by an increase of the built-in potential after solvent treatment due to the presence of interface dipoles. XPS/UPS results provide further evidence of the existence of interface dipoles by showing the energy-level alignment between the metal contact and organic material. Further studies for the interaction between the solvent treatment and the organic surface molecules are of interest and are under investigation.

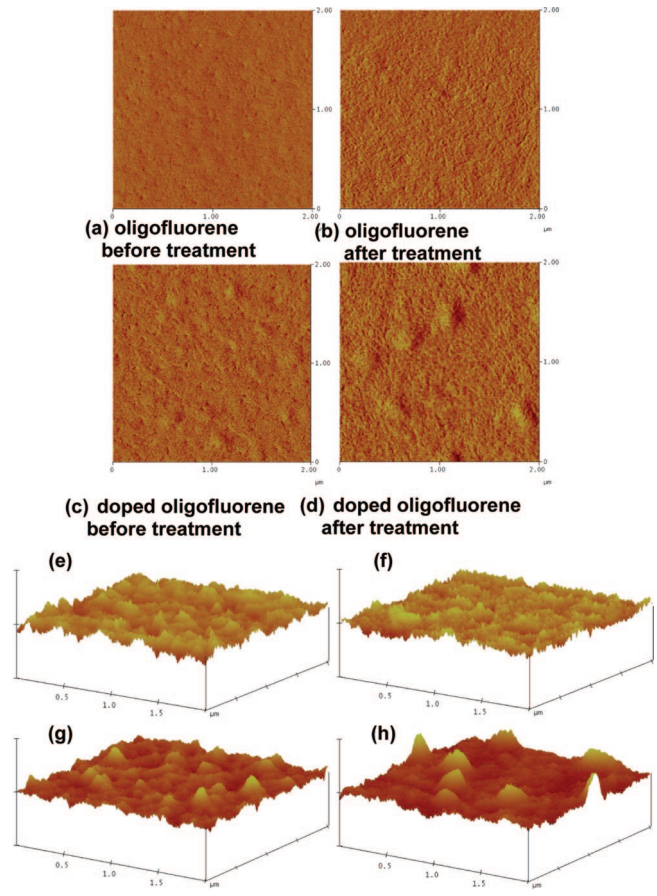

FIGURE 9. (a−d) AFM phase images of pure and doped oligofluorene before and after solvent treatment. (e−h) 3D images, respectively. The measured mean-square roughnesses (R_{rms}) are 0.98, 1.07, 1.27, and 1.91 nm, respectively, and data scales are 15, 20, 20, and 25 nm, respectively.

REFERENCES AND NOTES

(1) Baldo, M. A.; O'Brien, D. F.; You, Y.; Shoustikov, A.; Sibley, S.; Thompson, M. E.; Forrest, S. R. *Nature* **1998**, *395*, 151.
(2) Kawamura, Y.; Goushi, K.; Brooks, J.; Brown, J. J.; Sasabe, H.; Adachi, C. *Appl. Phys. Lett.* **2005**, *86*, 071104.
(3) Huang, J.; Watanabe, T.; Ueno, K.; Yang, Y. *Adv. Mater.* **2007**, *19*, 739.
(4) Lan, P. A.; Palilis, L. C.; O'Brien, D. F.; Giebeler, C.; Cadby, A. J.; Lidzey, D. G.; Campbell, A. J.; Blau, W.; Bradley, D. D. C. *Phys. Rev. B: Condens. Matter Mater. Phys.* **2002**, *63*, 235206.
(5) Vaeth, K. M.; Tang, C. W. *J. Appl. Phys.* **2002**, *92*, 3447.
(6) Gong, X.; Robinson, M. R.; Ostrowski, J. C.; Moses, D.; Bazan,

G. C.; Heeger, A. J. *Adv. Mater.* **2002**, *14*, 581.
(7) Choulis, S. A.; Choong, V.-E.; Mathai, M. K.; So, F. *Appl. Phys. Lett.* **2005**, *87*, 113503.
(8) Nakayama, T.; Hiyama, K.; Furukawa, K.; Ohtani, H. *Dig. Tech. Pap.—Soc. Inf. Disp. Int. Symp.* **2007**, *38*, 1018.
(9) Tsujimura, T.; Zhu, W.; Mizukoshi, S.; Mori, N.; Miwa, K.; Ono, S.; Maekawa, Y.; Kawabe, K.; Kohn, M. *Dig. Tech. Pap.—Soc. Inf. Disp. Int. Symp.* **2007**, *38*, 84.
(10) (a) Klessinger, M.; Michl, J. *Excited States and Photochemistry of Organic Molecules*; VCH: New York, 1995. (b) Baldo, M. The Electronic and Optical Properties of Amorphous Organic Semiconductor. Ph.D. Dissertation, Princeton University, Princeton, NJ, 2001.
(11) Chen, F.; He, G.; Yang, Y. *Appl. Phys. Lett.* **2003**, *82*, 1006.
(12) Huang, J.; Xu, Z.; Yang, Y. *Adv. Funct. Mater.* **2007**, *17*, 1966.
(13) (a) Kamatani, J.; Okada, S.; Tsuboyama, A.; Takiguchi, T.; Miura, S.; Noguchi, K.; Moriyama, T.; Furigori, M. U.S. Patent 6,953,628, 2005. (b) Kamatani, A.; Okada, S.; Takiguchi, T.; Kurokawa, S. JP2006151888, 2006.
(14) Brown, T. M.; Kim, J. S.; Friend, R. H.; Cacialli, F.; Daik, R.; Feast, W. *J. Appl. Phys. Lett.* **1999**, *75*, 1679.
(15) Campbell, I. H.; Hagler, T. W.; Smith, D. L.; Ferraris, J. P. *Phys. Rev. Lett.* **1996**, *76*, 1900.
(16) Brown, T. M.; Friend, R. H.; Millard, I. S.; Lacey, D. J.; Butler, T.; Burroughes, J. H.; Cacialli, F. *J. Appl. Phys.* **2003**, *93*, 6159.
(17) Ishii, H.; Sugiyama, K.; Ito, E.; Seki, K. *Adv. Mater.* **1999**, *11*, 605.
(18) Salaneck, W. R.; Stafström, S.; Brédas, J. L. *Conjugated Polymer Surfaces and Interfaces: Electronic and Chemical Structure of Interfaces for Polymer Light Emitting Devices*; Cambridge University Press: Cambridge, U.K., 1996.
(19) Lu, B.; Zhang, H. J.; Li, H. Y.; Bao, S. N.; He, P. *Phys. Rev. B* **2003**, *68*, 125410.
(20) Kim, S. Y.; Baik, J. M.; Lee, J. *Electrochem. Solid-State Lett.* **2005**, *8*, H79.
(21) Yan, L.; Gao, Y. *Thin Solid Films* **2002**, *417*, 101.
(22) Niu, Y. H.; Jen, A. K.-Y.; Shu, C. *J. Phys. Chem. B* **2006**, *110*, 6010.

AM8000133